Journal of Constructional Steel Research 151 (2018) 194–203

Contents lists available at ScienceDirect

Journal of Constructional Steel Research

Seismic performance of a repaired thin steel plate shear wall structure

Yipeng Du, Jiping Hao *, Jinguang Yu, Haisheng Yu, Bowen Deng, Danlan Lv, Zhaoyang Liang

School of Civil Engineering, Xi'an University of Architecture & Technology, Xi'an 710055, China

ARTICLE INFO

Article history:
Received 26 June 2018
Received in revised form 6 September 2018
Accepted 20 September 2018
Available online xxxx

Keywords:
Steel plate shear wall
Multi-ribbed grid
Pseudo-static test
Post-reinforced performance

ABSTRACT

A multi-ribbed grid of channels can effectively restrain the deformation of an embedded steel plate shear wall, improving the elastic stiffness of the overall structure while enhancing its energy dissipation capacity. Aone-bay, two-story specimen was tested under low cycle reversed loading in two stages. After being damaged in Stage I, the structure was repaired by anchoring the multi-ribbed channel grid. The structure was then loaded to destruction. To investigate the changes in performance of the structure due to reinforcement, comparison and analysis of the structure were conducted for the two stages. The results indicate that in the elastic stage, when the repaired structure is in its normal service state, the deformation of the steel plate is effectively restrained, and the elastic stiffness and energy dissipation capacity is improved. In the elastic-plastic stage, the failure mode of the structure is reasonable, and the hysteresis loop is full as the multi-ribbed channel grid effectively restrains the pinching phenomenon. Based on the results of the experiment, finite element models were established. According to the finite element analysis, the yield load, initial stiffness, and maximum lateral force bearing capacity of the repaired structure improved significantly.

1. Introduction

The reinforcement of damaged structures represents a remarkable interest topic in the field of Seismic Engineering [1,2]. The steel plate shear wall structure is mainly composed of steel frames and embedded steel plates. The steel frame bears the vertical load while the embedded steel plate bears most of the horizontal load [3–4]. According to the "strong frame, weak wallboard" design concept, the embedded steel plate yields firstly and the frame yields secondly under an earthquake. [5–6]. This disaster prevention design concept makes the steel plate shear wall a repairable structure [7].

To determine the performance characteristics of a repaired steel plate shear wall, Qu etal. conducted a two-stagepseudo-dynamic test on a full-scaletwo-story steel plate shear wall specimen [8]. Between the two stages of the test, the damaged steel plate shear wall structure was repaired by replacing the embedded steel plates. The test results indicated that the repaired structure behaved similarly to the original one, demonstrating that it is feasible to repair damaged post-earthquake shear wall structures by replacing the embedded steel plates. However, significant labor is required to replace the embedded steel plates in practical applications. Therefore, it remains necessary to develop an easier repair method.

To address the difficulties of repairing or replacing embedded steel plate shear walls, the anchoring of a multi-ribbed channel grid to the shear wall to repair a damaged steel plate shear wall is proposed in this paper. To verify the performance of this proposed system, a single-span, two-story shear wall specimen was tested under two stages of low-cycle reversed loading. In Stage I, earthquake damage was applied to the specimen. Then the damaged structure was repaired using the multi-ribbed grid. In Stage II, the repaired structure was again loaded to the point of damage. The mechanical behavior of the frame in the elastic phase of each stage was then analyzed and compared. The failure mode and hysteretic behavior of the repaired structure was also studied.

2. Experiment details

2.1. Specimen design

In order to study the seismic performance of a steel frame-thin plate shear wall structure before and after repair, a one-bay, two-story specimen was designed for a pseudo-static test based on typical building details. To accommodate the available test conditions, the geometric similarity ratio of the specimen was set to 1:3. The clear height of each story in the specimen was 1200 mm, making the total height of the specimen 3670 mm, and the center-to-center spacing of the columns was 1380 mm. The beam-to-column joints were welded without inner diaphragms.

To ensure that the frame effectively anchored the embedded steel plates so that the post-buckling strength of the steel plates could be fully utilized, 100 × 8 mm splice plates were butt welded to the frame and fillet welded to the embedded steel plate. To simulate the requirements of building infrastructure, which often must pass pipes through

* Corresponding author.
E-mail address: haojiping@xauat.edu.cn (J. Hao).

https://doi.org/10.1016/j.jcsr.2018.09.020
0143-974X/

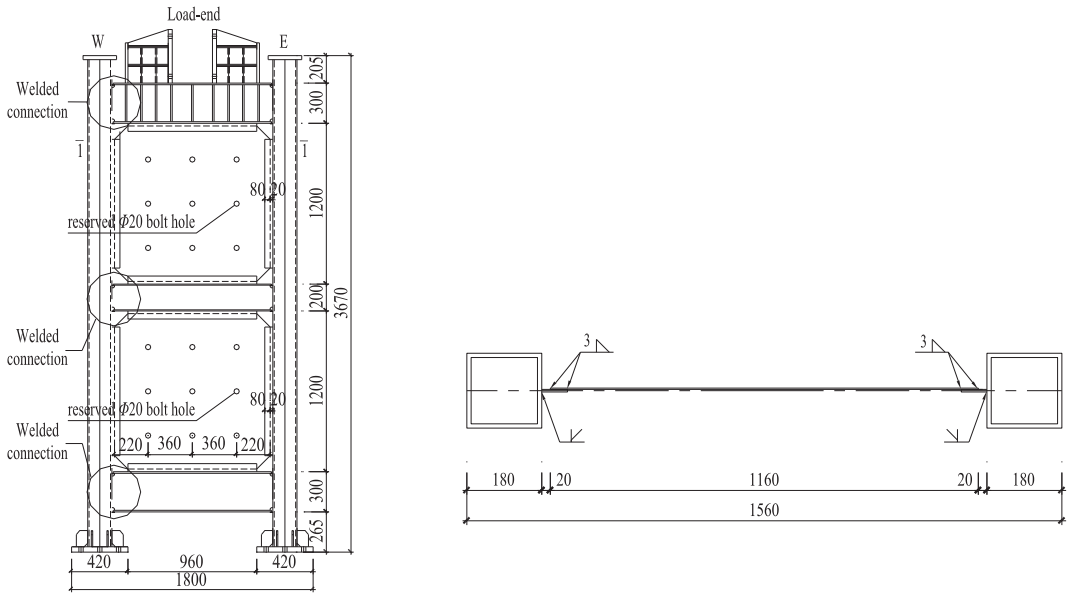

(a) Dimensional drawing (b) Section 1-1

Fig. 1. Dimensions of specimen (mm).

a shear wall, 100 mm was cut off of each corner of the embedded steel plate. Large 20-mm diameter bolt holes were included on the embedded steel plates to provide convenient installation of the multi-ribbed grid. The geometry of the specimen is shown in Fig. 1.

Following the conclusion of Stage I, the multi-ribbed channel grid was anchored to the embedded steel plates with friction-type high strength bolts to reinforce the specimen. In this application, the relatively high stiffness of the multi-ribbed channel grid eliminates the residual deformation of the embedded steel plate once installed. Details of the multi-ribbed channel grid are shown in Fig. 2.

According to the ANSI/AISC 341-16 standard, "Seismic Provisions for Structural Steel Buildings", the frame should remain elastic before the plastic properties of the embedded steel plate are fully engaged [9]. To meet this requirement, Q345 steel was selected as the column material and Q235 steel was selected for the remaining components, based on the results of a finite element analysis of the frame. To ensure the stability of the steel frame-thin plate shear wall structure in the out-of-plane direction, square steel tubes were selected as the column sections. The sections of each component are shown in Table 1.

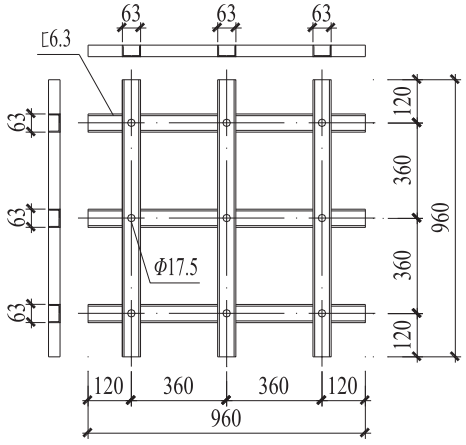

Fig. 2. Details of multi-ribbed channel grid (mm).

2.2. Test setup

Based on the test requirements, the lateral deformation and overall displacement of the specimen were monitored. To measure the horizontal displacement at each story of the specimen, displacement gauges were placed on the east and west sides of each beam. To measure the deformation of the columns, displacement gauges were placed on the columns in the middle of each story in the in-plane direction. To monitor the overall displacement of the rigid body, displacement gauges were placed at the column bases and the ground beam. Strain gauges were placed at the column bases, beam-column joints, and diagonally on the embedded steel plate [10] to monitor the changes in the stress during loading.

The experimental setup is shown in Fig. 3. The specimen was fixed to the ground beam by high-strength bolts. The ground beam was in turn thoroughly fixed to the ground by two support beams. Vertical loads were applied to the steel columns by two hydraulic jacks mounted on sliding bearings. The horizontal load was applied by two 1000-kNMTS hydraulic servo actuators with a stroke of ±250 mm to the top beam through a loading beam. Lateral braces were placed on both sides of the middle beam and the top beam, and they were connected to the specimen by wheels to reduce the influence of friction on the horizontal bearing capacity of the frame.

2.3. Material properties

The steel frame and embedded steel plates were sampled and tested according to [11–13]. The results are shown in Table 2.

Table 1
Sections of specimen.

Component	Section(mm)	Component	Section (mm)
Column	180 × 180 × 10	Splice plate	−100 × 8
Top and bottom beams	HN300 × 150 × 6.5 × 9	Embeddedsteel plate	−3
Middle beam	HN200 × 100 × 5.5 × 8	Channelstiffener	6.3

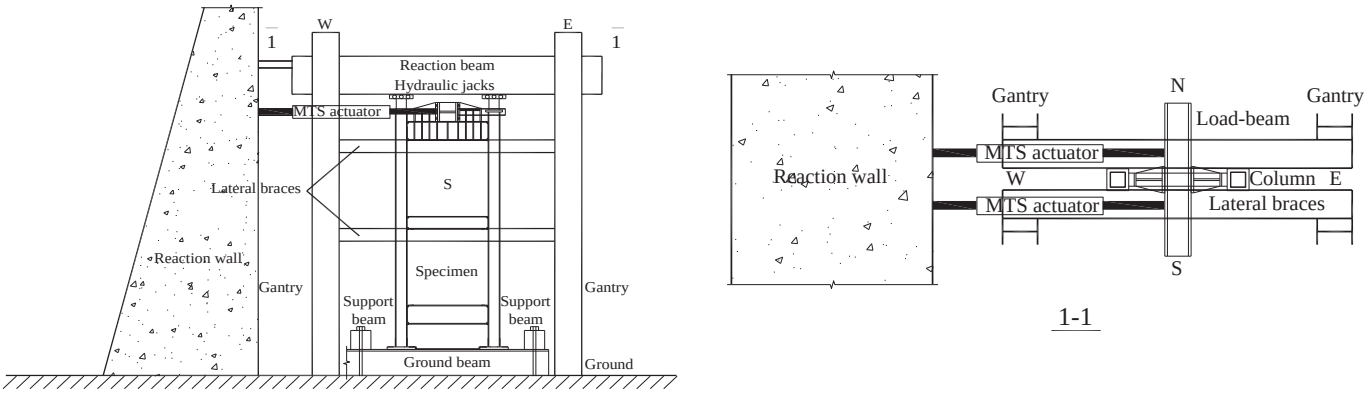

Fig. 3. Design of loading system.

2.4. Testing procedure

Referring to [14], the loading scheme was applied using displacement control mode to meet the test demand. Each load increment was applied one time before yielding, and three times after yielding. The required performance indices used to determine loading scheme were taken from [15], and are provided in Table 3.

Before commencing the displacement test in each stage, a vertical load constituting 25% of the axial compression capacity, or 580 kN to each column, was applied to the columns.

In Stage I, in order to ensure the uniformity and continuity of loading, the displacement load was applied in 5-mm increments. Once loaded to the target drift angle of 1/130, the structure was considered partially damaged and the experiment for Stage I was terminated. The specimen was then repaired by anchoring the multi-ribbed channel grid to the frame-plate assembly.

In Stage II, the repaired specimen was loaded in an applied displacement increment of 5 mm prior to yielding, and an applied displacement increment of $0.5\Delta y$, or 12.5 mm, after yielding. When the drift angle reached 1/50, the displacement of the specimen was regarded to have been subjected to one level of load. When the capacity of the specimen decreased to 85% of its maximum load capacity, the specimen was considered to be destroyed and the test was concluded. The loading scheme is shown in Fig. 4.

3. Experiment results

3.1. Experimental observations

There were no obvious phenomena observed during the initial vertical loading process. After the application of the vertical load, the instruments were checked before the horizontal loading stage was conducted.

In Stage I, the specimen was in the elastic state during the application of the first two levels. After the applied displacement reached 10 mm, the embedded steel plates were observed to have buckled, but this deformation disappeared when unloaded. When the horizontal displacement reached 15 mm, tension fields were clearly formed in the embedded steel plates, and, according to the strain gage data, the steel plates yielded. Once unloaded, residual deformation of the steel plates in both stories was observed in the form of the tension field. After the horizontal displacement had reached 25 mm (a drift angle of 1/130), the stress in the embedded steel plates continued to develop in the plastic state. The paint on the corners of the steel plates came off (Fig. 5(a)), and when unloaded, the residual deformation of the steel plates was obvious (Fig. 5(b)). The maximum out-of-plane residual deformation of the steel plates was about 30 mm. At this load, the outside of the column base yielded, and the area of the hysteresis loop increased slightly, indicating that the specimen had indeed entered the yielding stage.

At the conclusion of Stage I, the steel frame basically remained in the elastic state and the steel plate remained in the elastic-plastic state. Note that once the out-plane residual deformation of an embedded steel plate is greater than $(L \cdot h_s)^{1/2}/50$, the stiffness of the plate greatly decreases [16]. After Stage I of this experiment, the deformation of the steel plates was greater than this limit value. Therefore, repair was deemed necessary and the multi-ribbed channel grids were anchored to the steel plates to eliminate their residual deformation and reinforce them. The bolt holes of the embedded steel plates and the multi-ribbed channel grids caused misalignment in both in-plane and out-plane directions due to the previous loads. For easy assembly, M16 bolts with long bolt rod, smaller in size than bolt holes, were adopted in

Table 2
Results of tension coupon tests.

Sampling position	f_y (MPa)	f_u (MPa)	E (10^5 MPa)
Column	371.67	518.33	2.03
Top and bottom beam	316.67	550.00	2.01
Middle beam	290	398.33	2.00
Embedded steel plate	321.67	445.00	2.05

Table 3
Drift angle corresponding to seismic performance.

Performance level of structure				
Fully operational	Operational	Repair required	Life safety	Approaching collapse
1/300	1/230	1/130	1/90	1/50

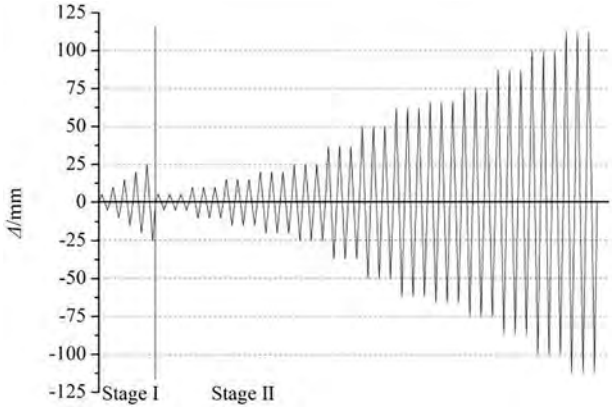

Fig. 4. Loading scheme.

Fig. 5. Phenomena in Stage I.

installation. After repair, the out-of-plane deformation of the embedded steel plates was about 2 mm. The repair process is shown in Fig. 6.

During the initial portion of the Stage II loading process, there were no obvious phenomena observed. The deformation of the steel plates was effectively restrained. At the $2.0\delta_y$ load level, the upper west corner of the steel plate cracked (Fig. 7(a)), and the welded connection point at the bottom flange of the bottom beam-to-column joint cracked. The data from the strain gauges indicated that the web of the middle beam had yielded. At the $2.5\delta_y$ load level, the deformation of the steel plates in each grid was obvious, and the cracks previously observed at the corner of the steel plate penetrated deeply into the plate (Fig. 7(b)), and the web plate in the middle beam was observed to buckle (Fig. 7(c)). The residual deformation of the steel plates was quite obvious once the specimen was unloaded. At this load level, the applied load on the specimen reached its maximum value of 794.3 kN. At the $2.64\delta_y$ load level (a drift angle of 1/50), the welded connection at the bottom flange of the bottom beam-to-column joint was torn apart (Fig. 7(d)), the entire section of the column yielded, and the column base buckled (Fig. 7(e)). At the $3.0\delta_y$ load level, the welded connection point at the bottom beam-column joint disconnected, and the top flange of the middle beam yielded on the east side. At the $4.0\delta_y$ load level, the load capacity of the specimen continued to decline, and the damage to the specimen increased further (Fig. 7(f)). When the $4.5\delta_y$ load level was applied, the capacity of the specimen declined to 85% of its maximum load capacity and the experiment was terminated. The final form of the destroyed specimen is shown in Fig. 7(g).

The performance and failure mode of the repaired structure are in line with general expectations. The pseudo-static test results of the repaired specimen indicate that anchoring the multi-ribbed channel grid can effectively eliminate the residual deformation of the steel plate and restrain the embedded steel plates in the post-repair condition. When the repaired structure was damaged in a reasonable sequence, it exhibited high ductility.

3.2. Experimental analysis

3.2.1. Hysteretic curves

The hysteresis curves from the specimen tests are shown in Fig. 8. In Stage I, the specimen is basically in the elastic state, and the load-displacement curve is linear when the displacement is less than 10 mm. With the increase in load level, the area of the hysteresis loop increases, and the embedded steel plate forms a tension field. By the conclusion of Stage I, the specimen begins to yield.

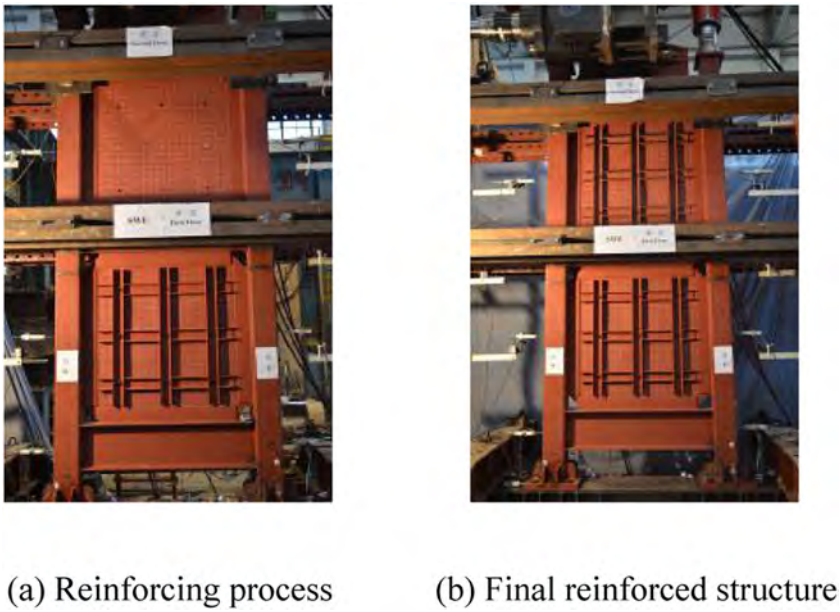

Fig. 6. Repair process.

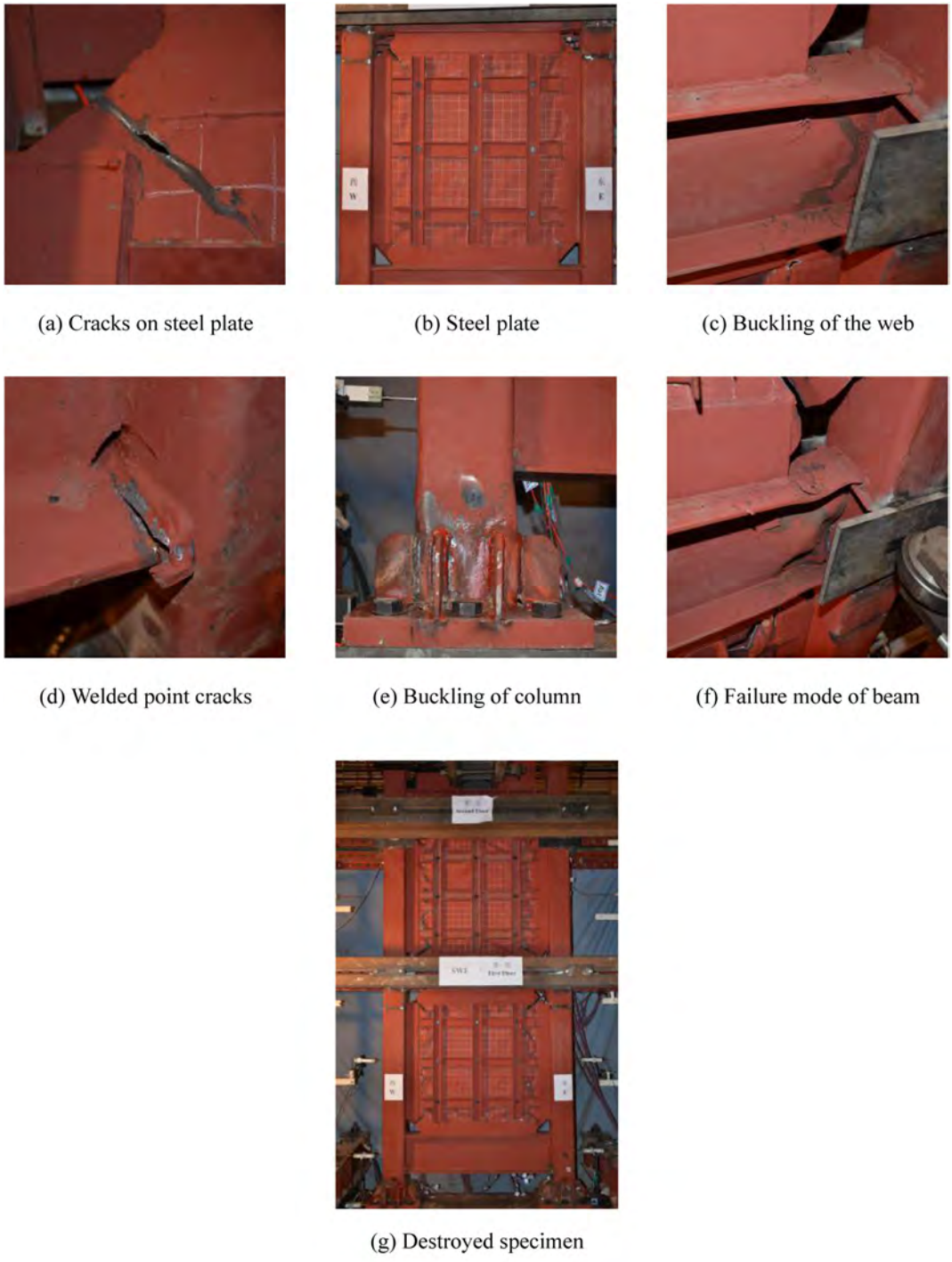

Fig. 7. Failure modes in Stage II.

At the beginning of Stage II, the area of the hysteresis loop is small, and the load-displacement curve is linear. There is no residual deformation in the steel plate when the specimen is unloaded between load applications. In the elastic stage, the load capacity of the repaired structure is higher than that of the original structure. With the increase in applied load, the stiffness of the structure, provided mainly by the embedded steel places and the steel frame, decreases, and so the area inside the hysteresis loop increases. At this time, the hysteresis loop is quite plump. When the load level reaches 75 mm ($3\delta_y$), the stiffness and bearing capacity of the specimen obviously decrease, and the hysteresis loop becomes pinched. In the last load level, this pinching phenomenon is further exaggerated. When unloaded to zero displacement at this point, the stiffness of the structure is close to zero.

3.2.2. Skeleton curves

The skeleton curves of the specimen are shown in Fig. 9. The elastic stiffness of the repaired structure is clearly greater than that of the original structure. At the 25 mm load level, the secant stiffness of the ultimate bearing capacity point is 14% greater than that of the original structure, indicating that the stiffening of the embedded steel plate using the multi-ribbed channel grid effectively increases the stiffness of the original specimen. The yield displacement of the repaired

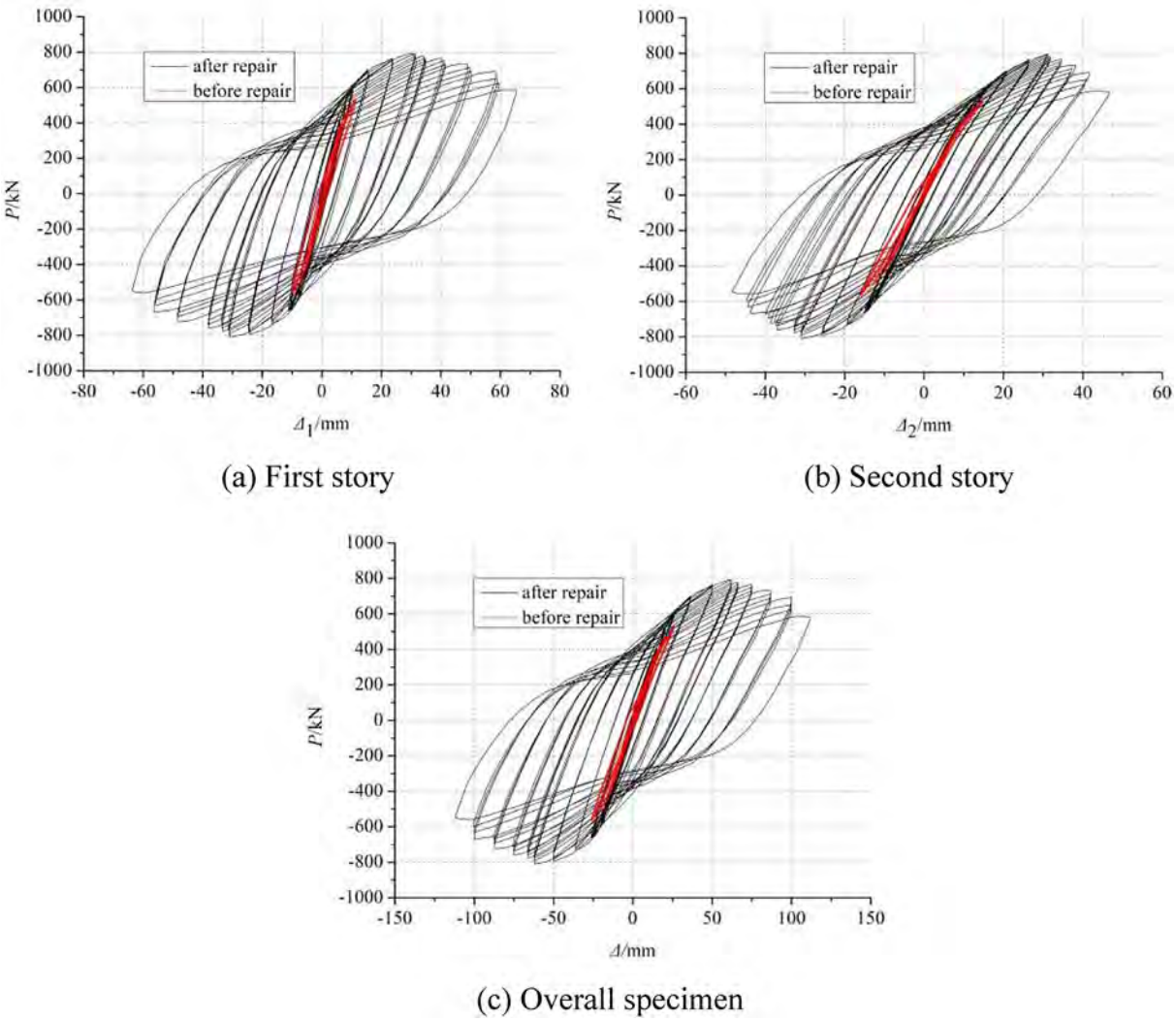

Fig. 8. Hysteresis curves.

structure is 30.5 mm, the yield load is 677.9 kN, the ductility coefficient is 3.12, and the ultimate displacement of the specimen is 108 mm. When the specimen reaches its maximum capacity, the skeleton curve decreases gently, indicating a ductile failure.

3.2.3. Capacity degradation

Capacity degradation is the loss of capacity between each load cycle under the same displacement. The capacity degradation curves are shown in Fig. 10. The variables λ_1 and λ_2 are the ratio of the capacity

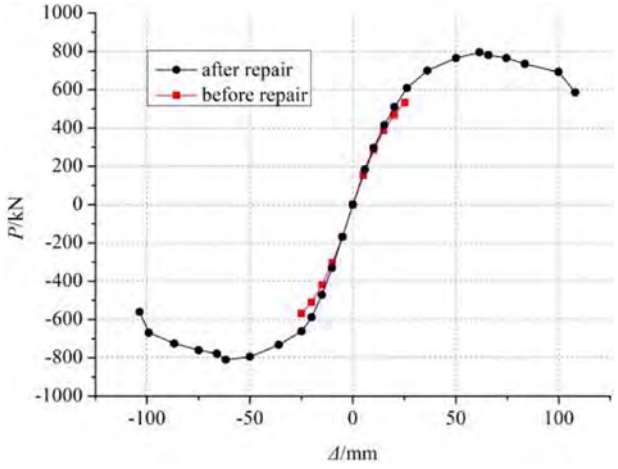

Fig. 9. Skeleton curve.

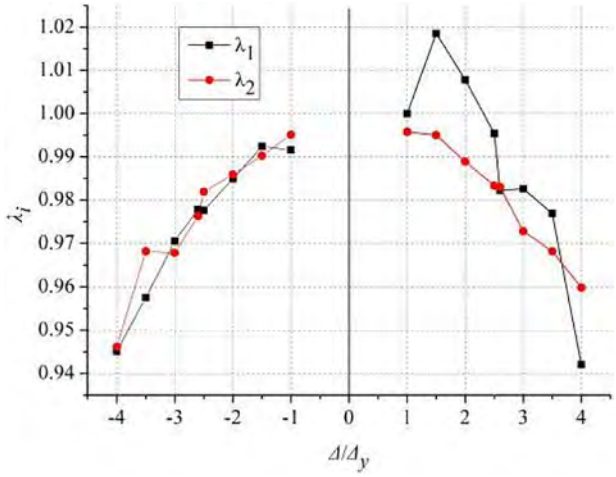

Fig. 10. Capacity degradation.

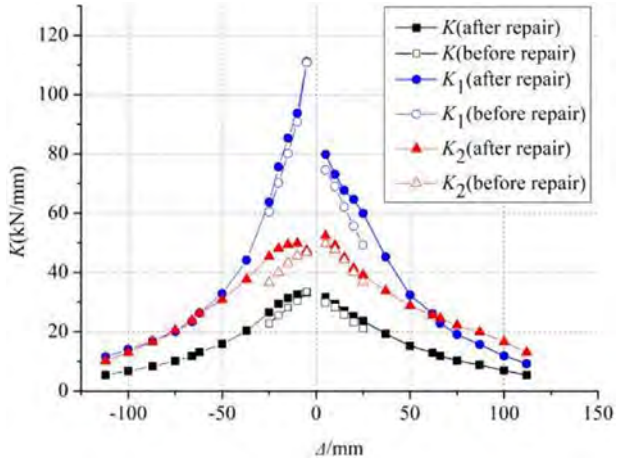

Fig. 11. Stiffness degradation.

of the first cycle to the capacity of the second cycle and the ratio of the capacity of the second cycle to the capacity of the third cycle, respectively. The coefficient of capacity degradation for the repaired specimens is greater than 0.94, indicating that the repaired structure provides superior internal force redistribution and stable capacity.

3.2.4. Stiffness degradation

The stiffness degradation characteristics of the specimen are evaluated using the secant stiffness of the peak load during the first cycle of each load level. As shown in Fig. 11, the installation of the multi-ribbed grid effectively improves the stiffness of the specimen. The initial elastic stiffness of repaired specimen is 32.5 kN/mm. The stiffness of the specimen then decreases gently. The final stiffness loss is 83% at specimen destruction. The initial stiffness of the first story is obviously greater than that of the second story. When the load level reaches $2.5\Delta_y$, a plastic hinge forms at the column base, and the restraint of the first story decreases accordingly, as reflected in the decrease of stiffness in the first story.

3.2.5. Energy dissipation capacity

The energy dissipation capacity is evaluated using the damping coefficient ζ:

$$\zeta = \frac{1}{2\pi} \cdot \frac{S_{(ABC+CDA)}}{S_{(OBE+ODF)}} \tag{1}$$

where $S_{(ABC+CDA)}$ is the area of the hysteresis loop and $S_{(OBE+ODF)}$ is the area of the triangle formed by the peak load and the axes [14]. As shown in Fig. 12, the energy dissipation capacity of the repaired structure is less than that of the original structure in the elastic state. In the elastic-plastic state, the energy dissipation capacity of the specimen rises. The average value of the damping coefficient ζ is 0.15 in the plastic state, which means that the energy dissipation capacity of the structure is good. The trend of the energy dissipation capacity indicates that the two stories of the specimen cooperate well during the loading process.

4. Numerical simulation

4.1. Finite element model establishment

To further study of the global behavior of the reinforced steel plate shear wall specimen, 3D finite-element models were developed in ABAQUS/Standard to simulate the responses of the specimen loaded under low cyclic reversed loading [17].The embedded steel plates, beams, and columns were modeled with a four-node, reduced integrated shell element S4R [18]. The effect of the bolts between the multi-ribbed channel grids and the embedded steel plates was simulated by a tie element. The multi-ribbed channel grid was anchored via a model change function in ABAQUS. The stiffeners that had not been activated during Stage I were reactivated in Stage II. Geometric initial defects were considered in the FE model. According to the measurement, the initial out-plane deformation of the steel plates of the first and second stories was 2 mm and 3 mm respectively. The first and third order buckling modes were superimposed as the initial geometric defects of the structure, which is coordinated with the measurement. The buckling modes are shown in Fig. 13.

The bilinear kinematical material model was adopted for steel. The von Mises yield criterion was used for this model, and the Bauschinger effect was considered under cyclic loading [19,20]. Yield strength, elastic modulus, etc. were based on the test results in Table 2. The FE model is shown in Fig. 14.

4.2. Validating the finite element model

To validate the results of finite element analysis, the load-displacement curves of the experiment and the FE analysis in Stage II are shown in Fig. 15. The load-displacement curve obtained by FE analysis agrees well with the expriment in the elastic and elastoplastic stages. During the destruction stage, however, the decrease in the load-displacement curve obtained by finite element analysis is not obvious. This is mainly because the degradation in the lateral bearing

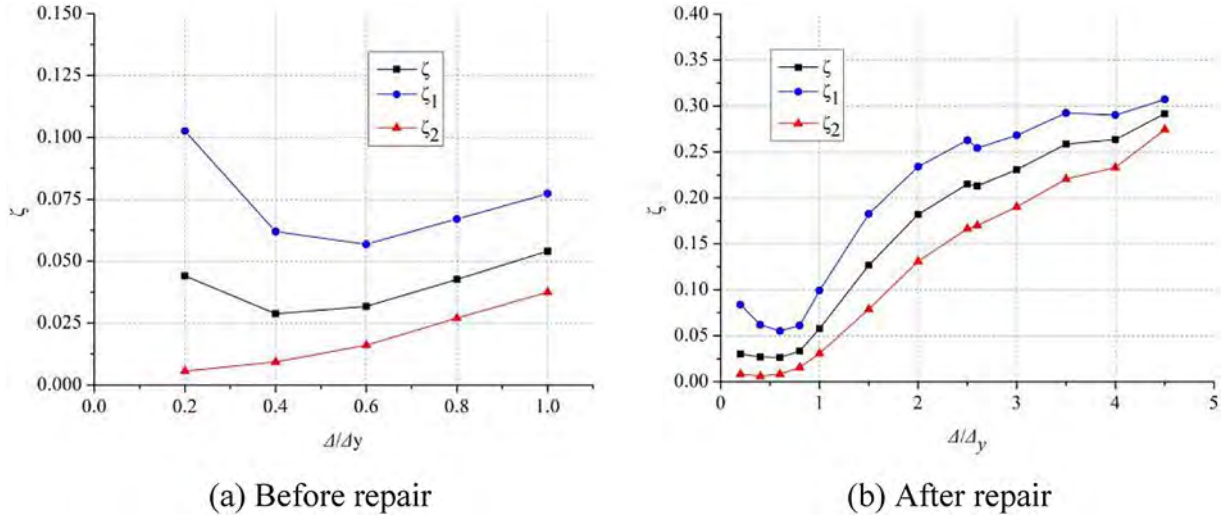

Fig. 12. Energy dissipation capacity.

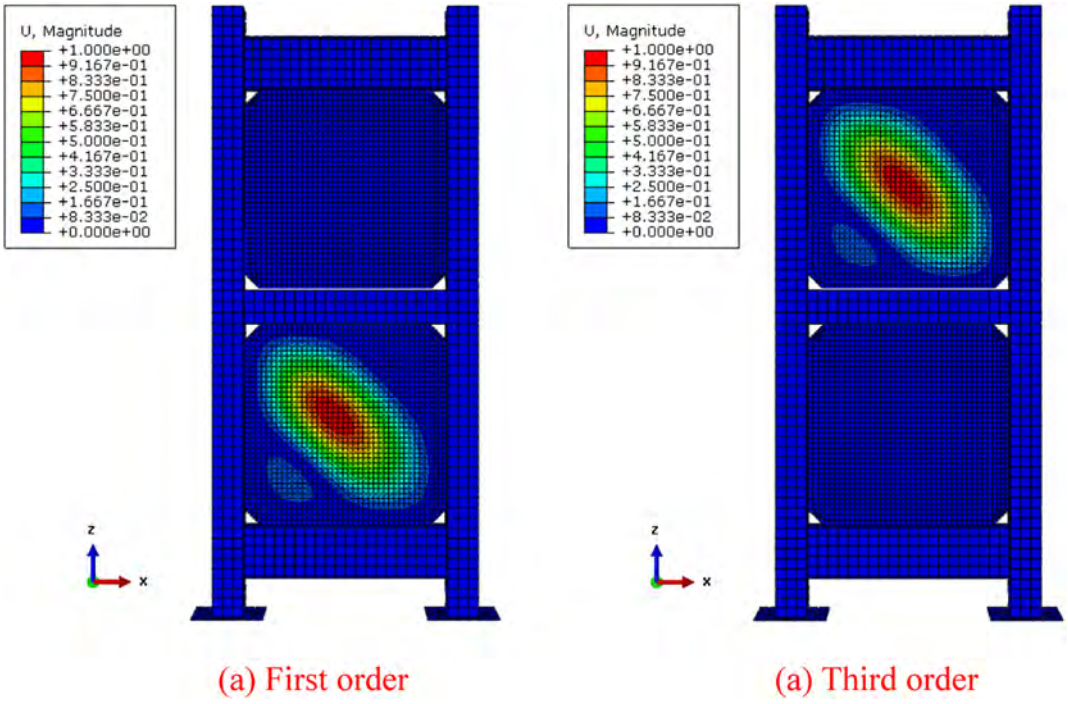

Fig. 13. Buckling modes.

capacity is partially due to the cracking of the welds connecting the embedded steel plates to the frame, or the beams to the columns [21,22].

The comparison between the experiment and finite element analysis results is shown in Table 4. The lateral load corresponding to the maximum displacement is about 98% of the peak load, and this does not meet the requirement of 85% of the maximum lateral force capacity. Therefore, the ultimate displacement of the finite element analysis results is taken as the same value as the experiment, and the ultimate lateral force capacity is taken as the load value corresponding to the maximum displacement. The deviation is defined as the ratio of the difference between the experiment result and the finite element analysis result to the test result. The deviation between yield loads and yield displacements is less than 3%, and the deviation between maximum loads and maximum displacements is less than 7%. The P_u of FE model is bigger than that of the experiment. It is mainly due to the ripping and fracture of the welds connecting either the embedded steel plates to the boundary frame, or the beam-column connections. In the present study, however, modeling of connection welds was not considered in FE model. In summary, the finite element model can accurately simulate the mechanical properties of the specimen in the elastic and elastoplastic stages and reveal the trend of the mechanical properties in plastic stage.

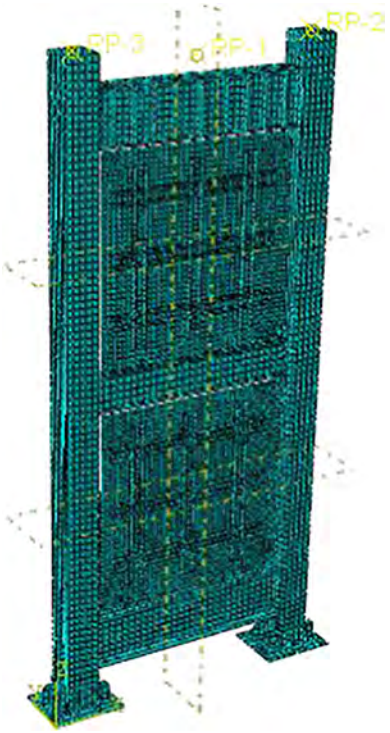

Fig. 14. Finite element model.

4.3. Comparison between the repaired and damaged structure

In this section, based on the finite element model of the specimen, the mechanical behavior of the repaired structure is compared to that of the damaged structure. Furthermore, the change in the mechanical

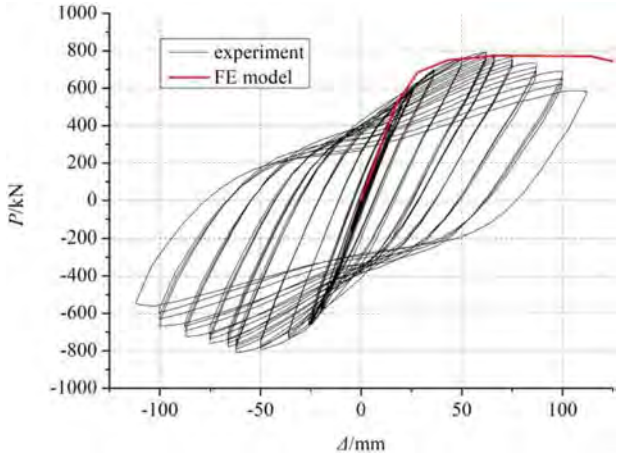

Fig. 15. Verification of the finite element model.

Table 4
Comparision between experiment and FE analysis.

	P_y (kN)	δ_y (mm)	P_{max} (kN)	δ (mm)	P_u (kN)	δ_u (mm)
Experiment	677.9	30.5	794.2	61.53	585.5	108
FE model	695.9	30.7	774.8	65.4	760.1	108.8
Deviation (%)	−2.7	−0.7	2.4	−6.3	−29.8	−0.7

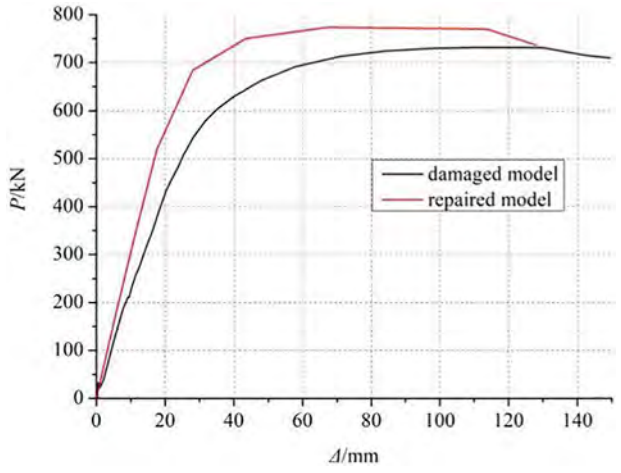

Fig. 16. Skeleton curves.

Table 5
Comparison of key data points between FE models.

	P_y (kN)	δ_y (mm)	K (kN/mm)	P_{max} (kN)
Repaired structure	695.9	30.7	22.7	774.8
Damaged structure	647.9	44.4	14.6	731.6
Increase rate (%)	6.9	–	35.7	5.6

properties of the specimens strengthened by the multi-ribbed grid is studied.

4.3.1. Mechanical properties analysis

The two FE models were applied with the same loading scheme which was used in the experiment. The damaged model was continuously loaded in two stages. And the repaired model was reinforced by the multi-ribbed grid after Stage I via the model change function in ABAQUS. To compare the mechanical properties of the repaired and damaged structure, the skeleton curves in Stage II of the two models were drawn in Fig. 16. The yield point and the maximum lateral load capacity point are shown in Table 5.

According to Table 5., the values of yield load, peak point load, and the initial stiffness of the structure reinforced by the multi-ribbed channel grid improved significantly compared with those of the damaged thin steel plate shear wall. By anchoring the multi-ribbed grid to the damaged thin steel plate shear wall, the lateral stiffness increased by 35.7%, the yield load by 6.9%, and the peak load by 5.6%.

4.3.2. Stress and deformation

The stress diagrams of the two models under a 1/50 drift ratio are shown in Fig. 17. The steel plate shear wall reinforced with multi-ribbed grids effectively reduces the additional bending moment of the frame, and it reduces the stress of the columns and beams, which effectively protects the steel frame from being destroyed. When the drift ratio reaches 1/50, the maximum out-plane displacement of the embedded steel plate reinforced by multi-ribbed grid is 3.3 mm, and that of the damaged steel plate is 33 mm, which indicates that the out-plane deformation of the steel plate reinforced by the multi-ribbed grid is effectively restrained.

5. Conclusions

In this research, a multi-ribbed channel grid was used to repair a damaged steel frame-thin steel plate shear wall structure. The behavior of the structure after repair was studied by experimental analysis. Based on the results of the experiment, finite element models were

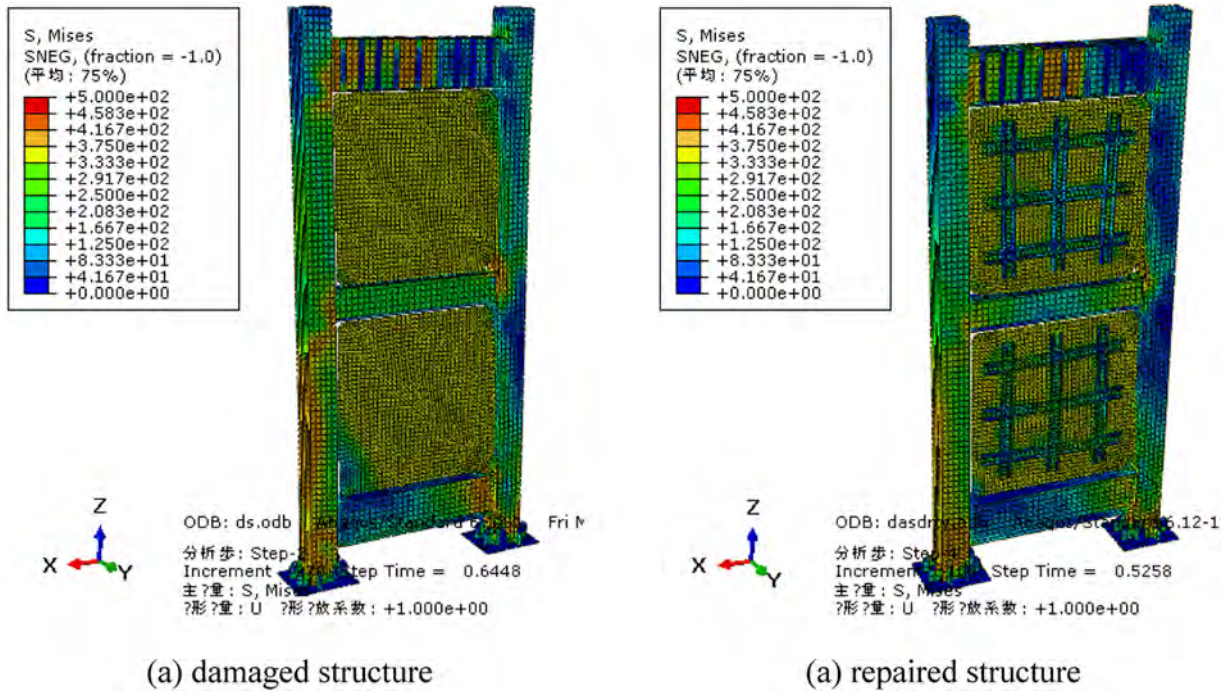

Fig. 17. Stress diagrams of each model under a drift ratio of 1/50.

established. Finally, the behavior of the repaired and damaged structure was studied. The conclusions of this research are as follows:

(1) The proposed method of anchoring a multi-ribbed channel grid to repair a thin steel plate shear wall structure can effectively reinforce the embedded steel plate and weaken the tension field effect.
(2) The failure mode of the post-repair structure is reasonable. The reinforced steel plate cooperated well with the partially yielded steel frame. The damaged steel frame beam ends and column bases were not destroyed prior to the reinforced embedded steel plate. Each panel of the embedded steel plate effectively resisted the lateral load and protected the steel frame. According to the FE analysis, the stress of the steel frame of the post-repair structure is smaller than that of the not repaired one at the drift ratio of 1/50.
(3) The multi-ribbed channel grid effectively restrains the out-plane deformation of the embedded steel plate and improves the energy dissipation capacity of the structure. The elastic stiffness of the post-repair structure is higher than that of the original structure. The hysteresis curve of the specimen is plump, and the redistribution of internal force is good. The average value of the damping coefficient ζ in the elastoplastic stage is 0.15.
(4) According to the finite element analysis, the yield load, initial stiffness, and maximum lateral force bearing capacity of the repaired structure improved significantly compared to those of the damaged structure. The multi-ribbed grids effectively reduced the out-plane deformation of the embedded steel plate, and reduced the additional bending moment of the frame. The repaired structure exhibited considerably better performance.

Acknowledgements

This paper was supported by the National Natural Science Foundation of China under Grant No. 51578442 and by the National Key Research and Development Program of China under Grant No. 2016YFC0701201.

References

[1] A. Formisano, G. De Matteis, F.M. Mazzolani, Numerical and experimental behaviour of a full-scaleRC structure upgraded with steel and aluminium shear panels, Comput. Struct. 88 (2010) 1348–1360.
[2] A. Formisano, F.M. Mazzolani, On the selection by MCDM methods of the optimal system for seismic retrofitting and vertical addition of existing buildings, Comput. Struct. 159 (2015) 1–13.
[3] J.W. Berman, M. Bruneau, Plastic analysis and design of steel plate shear walls, J. Struct. Eng. 129 (11) (2003) 1148–1156.
[4] L.J. Thorburn, G.L. Kulak, C.J. Montgomery, Analysis of steel plate shear walls, Structural Engineering Report, Vol. 107, University of Alberta, Canada, 1983.
[5] M. Elgaaly, Thin steel plate shear walls behavior and analysis, Thin-Walled Struct. 32 (1–3) (1998) 151–180.
[6] M. Ge, J. Hao, J. Yu, P. Yan, S. Xu, Shaking table test of buckling-restrained steel plate shear walls, J. Constr. Steel Res. 137 (2017) 254–261.
[7] A. Formisano, F.M. Mazzolani, Numerical analysis of slender steel shear panels for assessing design formulas, Int. J. Struct. Stab. Dyn. 7 (2) (2007) 1–22.
[8] B. Qu, M. Bruneau, C.H. Lin, K.C. Tsai, Testing of full-scaletwo-story steel plate shear wall with reduced beam section connections and composite floors, J. Struct. Eng. 134 (3) (2008) 364–373.
[9] ANSI/AISC, Seismic Provisions for Structural Steel Buildings, American Institute of Steel Construction, Chicago, IL, USA, 2016.
[10] M.J. Afshari, M. Gholhaki, Shear strength degradation of steel plate shear walls with optional located opening, Arch. Civ. Mech. Eng. 18 (2018) 1547–1561.
[11] GB/T 228.1-2010, Metallic Materials-TensionTesting-Part 1: Method of Test at Room Temperature, Standards Press of China, Beijing, 2010 (in Chinese).
[12] GB/T 2975-1998, Steel and Steel Products-Location and Preparation of Test Pieces for Mechanical Testing, Standards Press of China, Beijing, 1998 (in Chinese).
[13] G. De Matteis, G. Sarracco, G. Brando, Experimental tests and optimization rules for steel perforated shear panels, J. Struct. Eng. 123 (2016) 41–52.
[14] JGJ/T 101-2015, Specification for seismic test of buildings, China Architecture & Building Press, Beijing, 2015 (in Chinese).
[15] C.L. Fan, Study on Performance Based Seismic Design for Steel Frame-Steel Plate Shear Wall Structure, Ph.D. Thesis Department of Civil Engineering, Xi'an University of Architecture and Technology, Shaanxi China, 2014.
[16] M. Zhou, Studies on Design Method of Unstiffened or Buckling-Restrained Steel Plate Shear Wall Structures, Ph.D. Thesis Department of Civil Engineering, Tsinghua University, Beijing China, 2009.
[17] ABAQUS, Theory Manual, HKS Inc., USA, 2010.
[18] P.M. Clayton, C.Y. Tsai, J.W. Berman, et al., Comparison of web plate numerical models for self-centering steel plate shear walls, Earthq. Eng. Struct. Dyn. 44 (12) (2015) 2093–2110.
[19] H.C. Guo, J.P. Hao, Y.H. Liu, Behavior of stiffened and unstiffened steel plate shear walls considering joint properties, Thin-Walled Struct. 97 (1) (2015) 53–62.
[20] V. Caccese, M. Elgaaly, R. Chen, Experimental study of thin steel-plate shear walls under cyclic load, J. Struct. Eng. 119 (2) (1993) 573–587.
[21] R.G. Driver, G.L. Kulak, D.J. Laurie Kennedy, A.E. Elwi, Cyclic test of four-story steel plate shear wall, J. Struct. Eng. ASCE 124 (2) (1998) 112–120.
[22] A.S. Lubell, H.G.L. Prion, C.E. Ventura, M. Rezai, Unstiffened steel plate shear wall performance under cyclic loading, J. Struct. Eng. 126 (4) (2000) 453–460.